SCIENTIFIC REPORTS

OPEN

Electrochemical gating-induced reversible and drastic resistance switching in VO_2 nanowires

Received: 04 August 2015
Accepted: 26 October 2015
Published: 20 November 2015

Tsubasa Sasaki, Hiroki Ueda, Teruo Kanki & Hidekazu Tanaka

Reversible and drastic modulation of the transport properties in vanadium dioxide (VO_2) nanowires by electric field-induced hydrogenation at room temperature was demonstrated using the nanogaps separated by humid air in field-effect transistors with planer-type gates (PG-FET). These PG-FETs allowed us to investigate behavior of revealed hydrogen intercalation and diffusion aspects with time and spatial evolutions in nanowires. These results show that air nanogaps can operate as an electrochemical reaction field, even in a gaseous atmosphere, and offer new directions to explore emerging functions for electronic and energy devices in oxides.

The transport characteristics of transition metal oxides are sensitive to redox reactions because the valence numbers of the transition metal ions are easily changed by the reactions, which affect the carrier density and/or stabilization of the crystal structure[1–4]. Of the prototypical materials, VO_2 is promising as it undergoes a metal-insulator transition (MIT) and the resistance changes by orders of magnitude around 340 K. In VO_2 nano to microstructures[5–13], the coupling of the MIT with mechanical[7–9], optical[13], thermal[12] and electronic properties[9,11] can be used in tunable resonators, optical switchers, electronic and thermo-sensing devices. Furthermore, only a few atomic percent of the hydrogen- or oxygen-intercalation and -desorption in VO_2 cause drastic changes in the transport properties, equal to that caused by inducing the MIT[14–20]. Conventionally, controlling the amount of hydrogen/oxygen ions in an oxide has been conducted by annealing the samples under redox gas atmospheres[1,4,15,16], in an aqueous solution[17,18] and with a hydrogen spillover method[14,19]. Every method requires high temperatures of at least 150 °C. Recently, on the other hand, an electric field has been shown to be a means of both hydrogenation and oxidization in oxides at room temperature[20–23]. For example, a strong electric field in ionic liquid (IL) gates induces oxygen vacancy formation in VO_2[22]. In IL or CAN (amorphous $12CaO{\cdot}7Al_2O_3$ with a nanoporous structure) gates including water[21,24], furthermore, hydrogen ions can be intercalated by positive electric field. Thus electrochemical gating including water electrolysis has a full potential to allow tuning of doping level at room temperature. In this paper, we report investigation of systematic transport modulation in VO_2 nanowires by electrochemical gating *via* air gap under humid condition and establishment of the ion diffusion model, giving the hydrogen ion intercalation and diffusion aspects with time and spatial evolutions in VO_2.

Results

Proposed device structure. As a proper device structure to perform this experiment, we have prepared planer-type field effect transistor with side gates and a nanoscaled wire channel separated by air nanogaps (PG-FET) illustrated in Fig. 1a. This type of device has following advantages: An electric field can be applied under various different gas and vapor atmospheres through the air nanogap. In this study, air with various humidity levels and dry air were used. Secondly, the electric-field induced ion intercalation and diffusion aspects with the time and spatial evolutions in the vicinity of interface can be systematically investigated because ions are intercalated from channel edges of both side and diffuse

Institute of Scientific and Industrial Research, Osaka University, 8-1 Mihogaoka, Ibaraki, Osaka, 567-0047, Japan. Correspondence and requests for materials should be addressed to T.K. (email: kanki@sanken.osaka-u.ac.jp) or H.T. (email: h-tanaka@sanken.osaka-u.ac.jp)

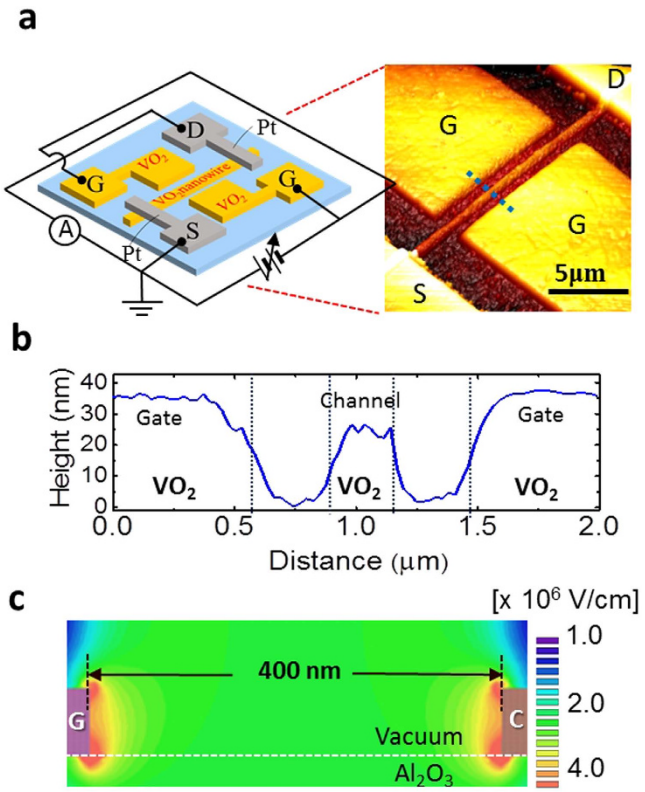

Figure 1. VO_2 nanowire device with planer-type gates. (**a**) The typical device architecture and an atomic force microscope (AFM) image of the VO_2 channel area. S, D and G indicate the source, drain and gate electrodes, respectively. (**b**) Cross-sectional AFM image, taken at the blue dashed line in (**a**). (**c**) Cross-sectional electric field map, determined using finite element analysis at $V_G = 100$ V through the 400-nm vacuum gap between G and the channel (**c**) on an Al_2O_3 substrate under vacuum.

from the sides in VO_2. Especially a narrower channel often enhances interface effect. An atomic force microscope image of a device is shown in Fig. 1a and the height profile is in Fig. 1b. The thicknesses of the channels and the gap distance were roughly 35 nm and 400 nm, respectively. The channel widths (w) were systematically changed from 3 μm to 400 nm (see Methods and Supplementary Information section A for details). Figure 1c shows a cross-sectional electric field-map, obtained using a Finite Element simulation using typical experimental parameters (see Supplementary Information section B). The electric field converged at the edges of the channels, providing the strongest effect on the electrochemical reactions. Thus the field-induced ion intercalation begins at the lateral sides of the nanowires

Drastic resistance modulation by electrochemical induced-hydrogenation. Figure 2a shows the reversible and non-volatile resistance modulation in a VO_2 nanowire channel ($w = 500$ nm), found by applying a positive and negative V_G at 300 K under a humidity of around 50%. The normalized resistance (R/R_0), where R and R_0 are the resistance and the pristine resistance before applying a V_G at 300 K, respectively, slowly continued to drop during the application of $V_G = +100$ V down to the saturation line at roughly $R/R_0 = 0.75$. This state was held after removal of the V_G. Namely, it exhibited a non-volatile memory effect. In contrast, the resistance increased again at $V_G = -100$ V. Regarding slow resistive drops by an electric field, it is suggested that the origin would be related to mechanical relaxation or slow traps according to some reports[25–27]. In our PG-FET devices, on the other hand, such slow changes in the resistance were not observed under dry air condition (Fig. 2b). A steep resistance-switching of 0.06% occurred without any non-volatile memory effects, as shown in the inset of Fig. 2b. Approximately 10^{12} cm^{-2} electrons should be accumulated at $V_G = 100$ V and 400 nm-gap distance. From Hall measurements in VO_2 thin films on Al_2O_3 substrates[28], the carrier density was evaluated at ~4×10^{18} cm^{-3}, equivalent to the Debye length of ~2 nm. Given modulation of resistivity in both lateral sides in our device geometry, the calculated modulation rate would be ideally 0.4%. Thus, it is considered that a pure carrier accumulation acts at lateral sides in dry air condition though the efficiency on the electrostatic effects was not so high compared with the ideal case. From the presence of the steep resistive switching in Fig. 2b, the origin of slow resistive drops under humid air conditions is not likely to attribute to the mechanical relaxation or slow traps as mentioned above, but rather to electrochemical reaction with intercalation of hydrogen ions[21,24,27,29], which can significantly reduce resistivity in 3d-orbital sensitive systems[30] (see Supplementary

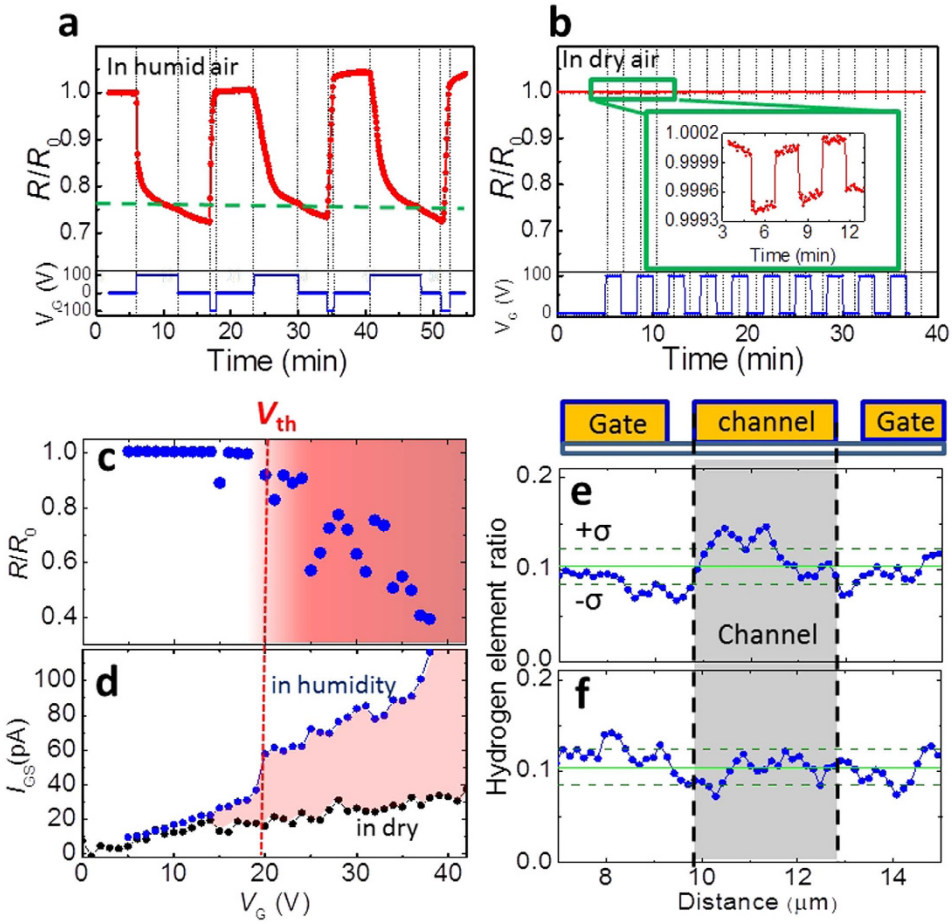

Figure 2. Effect of the electric field on the transport properties and hydrogen intercalations in a VO_2 channel. (**a**,**b**) Time dependence of the normalized resistance (R/R_0, where R_0 is the pristine resistance of a non-treated VO_2 channel at 300 K with applied V_G values of 100, 0 and −100 V) (**a**) in humid air and (**b**) in dry air. The green dashed line in (**a**) indicates the rough saturation of R/R_0. The inset in (**b**) is a magnified view. (**c**) V_G dependence of R/R_0 after applying a V_G for 20 minutes. (**d**) V_G dependence of the current between the gate and source electrodes (I_{GS}) under a humidity of 60% (blue dotted-line) and in dry air (black line). (**e**,**f**) The relative elemental ratios for hydrogen normalized by oxygen (**e**) in a device after applying $V_G = 100$ V and (**f**) in a pristine device. The solid and dashed green lines represent the averages of the hydrogen atom profiles and the standard deviations, respectively.

Information C for the intercalation ($V_G = 100$ V) and non-intercalation ($V_G = 0$ V) cases in detail) and/or color-switching properties known as electrochromism[31]. In VO_2 intercalated hydrogen ions, a strong H-O bond induces electron transfer from hydrogen onto the oxygen atom, resulting in higher 3*d*-orbital occupancy of vanadium from $V^{4+}(3d^1)$ to $V^{3+}(3d^2)$[5]. Figure 2c shows V_G dependence of R/R_0 20 minutes after applying the V_G to investigate the magnitude of resistance changes with variety of V_G. The threshold voltage starting to the reduction (V_{th}) was approximately 20 V and the magnitude of the resistance changes was enhanced with increasing V_G. The resistance fluctuation in over 20 V would be due to fluctuation for level of humidity. The resistance modulation is sensitive to the level of humidity. In addition, repetitive intercalation and desorption of hydrogen ions may slightly change crystallinity of VO_2 channels, causing the resistive fluctuation. In response with the resistance changes, the current between the gate and source electrodes (I_{GS}) suddenly increased at around 20 V as seen in Fig. 2d, corresponding to the V_{th} in Fig. 2c. Subtracting the current recorded under humid conditions from that recorded under dry conditions gives the current generated by the electrolysis of water. Accordingly, the density of generated hydrogen ions increases with increasing V_G and the number of intercalated hydrogen ions in VO_2 increases. Additionally, Fig. 2e shows the ratio of hydrogen elements in a device after applying $V_G = 100$ V, investigated by ToF-SIMS (time-of-flight secondary ion mass spectrometer). It can be indicated that hydrogen content in VO_2 channel is higher than that in other area in a device after applying the V_G, though the hydrogen content is roughly averaged because spatial resolution in the measurement is several hundred nanometer at most, whereas the hydrogen contents remain unchanged in a pristine device in Fig. 2f (see Supplementary Information section D in detail).

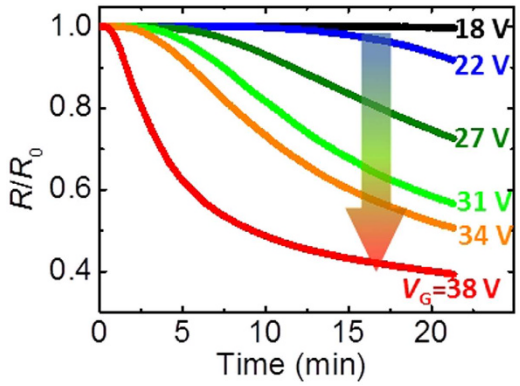

Figure 3. Transport properties from redox reactions in VO_2 by the electrolysis of water with various V_G values. Time dependence of R/R_0 for different V_G values under a humidity of 60% at 300 K.

Establishment in ion diffusion model by electrochemical gating. It is known that a 1% hydrogen intercalation per VO_2 unit cell induces almost one order of magnitude reduction in resistivity[17,18]. Based on the empirical facts and the intercalation from the channel edge by applying electric gate from lateral sides, the amount of intercalated hydrogen ions and the effect on the diffusive aspect in VO_2 can be evaluated by investigating the resistive behavior with a variety of V_G values. Figure 3 shows the time dependence of the resistive modulations with various V_G under a humidity of 60%. The resistance began to decrease above $V_G = 22$ V, approximately corresponding to the V_{th}. In the characteristic features, the magnitude of resistance reduction rate increases with increasing V_G and the initial reduction speed is faster in the larger V_G, while the reduction speed became slower with time.

To understand such transport behaviors in a variety of V_G, theoretical investigations have been carried out with a combination of chemical reaction kinetics at the interface and ion diffusion model under an electric field[32]. The external hydrogen ions stochastically react with VO_2 at the interface. The reaction rate depends on the external hydrogen ion concentration (n_{H+}) generated by electrolysis of the absorbed water. The n_{H+} tends to increase with increasing current between the gate and channel electrodes (I_{gc}^{ER}), promoting formation of HVO_2. While at the same time, desorption of hydrogen, namely return to VO_2, would occur because of the natural recovery of resistivity by the thermal energy as seen in Supplementary Information section E. Thus assuming the reversible reaction, the time evolution-dependence of the concentration of intercalated ions inside VO_2 at the interface (n_{inter}) can be written as a differential equation with respect to time (t):

$$\frac{dn_{\text{inter}}}{dt} = k_1 n_{\text{H+}} - k_2 n_{\text{inter}} \tag{1}$$

where k_1 and k_2 are the forward and reverse reaction rate constants, depending on the activation energy at the interface and temperature. Next, we consider how the intercalated ions diffuse in VO_2. Theoretically, for ion diffusion, the ionic fluxes likely arise from the gradients of the ion concentration and the electric gradients in solid-state materials[32]. Thus, as n_{HVO2} is the hydrogen ion concentration in VO_2, the hydrogen ion flux (J_{HVO2}) can be described as: $J_{HVO2} = -D\nabla n_{HVO2} + \mu E n_{HVO2}$, where D is the diffusivity, μ is the mobility and E is the internal electric field in VO_2. The first and second terms represent ion diffusion by the ion concentration gradient and by an electric field, respectively. The E resulting from V_G is screened by mobile electrons in VO_2 according to Poisson's equation, given as a function of the distance (x) from the interface ($x = 0$), namely, $E(x) = \frac{eN_0}{\varepsilon_0\varepsilon_r}(x_0 - x)$, where e is the elementary charge, N_0 is the carrier density in VO_2, and ε_r and ε_0 are the relative permittivity of VO_2 and the permittivity of a vacuum, respectively. x_0 can be expressed as: $\frac{\varepsilon_0\varepsilon_r}{eN_0}\frac{V_G}{d}$ as a function of V_G, where d is the distance between the gate and channel. N_0 and ε_r change with depending on the magnitude of intercalated hydrogen ions, however, N_0/ε_r can be treated as a constant value because the change rate of ε_r is roughly proportional to that of N_0[33]. Thus, the length of x_0 would be determined only by the magnitude of V_G, and E linearly decreases as a function of x and become zero at x_0, as shown in Fig. 4a. To conduct the unsteady state analysis, we use Fick's second law in the one dimensional case, namely, $\frac{\partial n_{HVO2}}{\partial t} = -\frac{\partial J_{HVO2}}{\partial x}$, which predicts the time and spatial evolutions of the ion concentration. With this the following equation was obtained:

$$\frac{\partial n_{HVO2}}{\partial t} = -D\frac{\partial^2 n_{HVO2}}{\partial x^2} + \frac{e\mu N_0}{\varepsilon_r\varepsilon_0}\{n_{HVO2} - (x_0 - x)\}\frac{\partial}{\partial x}n_{HVO2} \tag{2}$$

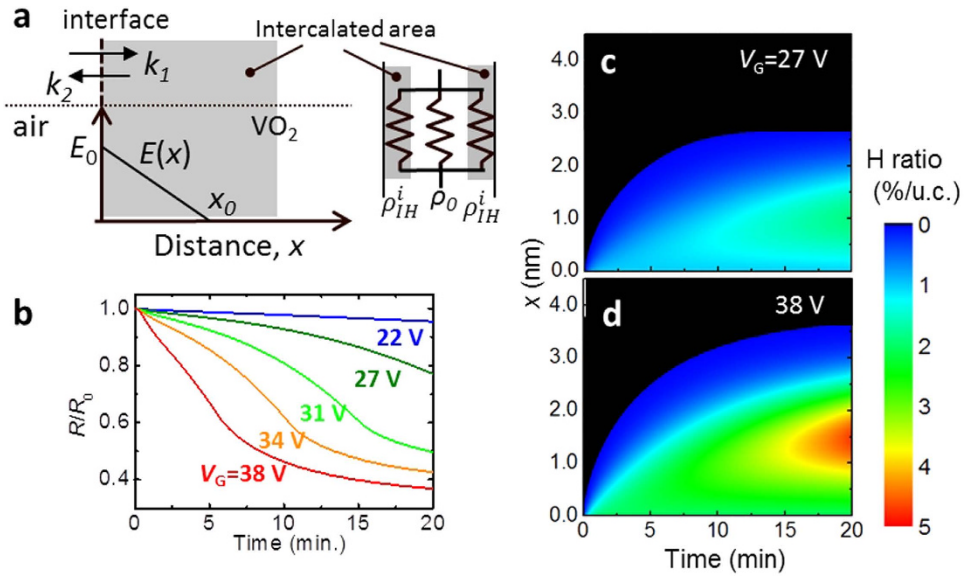

Figure 4. Simulated transport properties determined by the diffusion of intercalated ions. (**a**) Schematic of the ion intercalation at the interface between air and VO_2, resulting from chemical kinetics and the diffusion area (gray region), found using Fick's diffusion model under an electric field ($E(x)$) derived by Poisson's equation. The simulated channel resistance was calculated using the parallel resistor model for the intercalated (ρ_{IH}) and non-intercalated (ρ_0) resistivities and by taking each width into consideration, as shown on the right side in (**a**). (**b**) Time dependence of the simulated R/R_0 with a variety of V_G values for 500 nm wide VO_2 channels. (**c**,**d**) Spatial- and time-evolution maps of the hydrogen ion concentration at (**d**) $V_G = 27$ V and (**e**) 38 V. $x = 0$ indicates the interface.

Furthermore, using a parallel resister model for the resistivity in the intercalated (ρ_{IH}) and non-intercalated (ρ_0) parts in Fig. 4a and assuming a 1% hydrogen intercalation per VO_2 unit cell induces one order of magnitude reduction in the resistivity[17,18], R/R_0 could be evaluated as the following equation:

$$\left(\frac{R}{R_0}\right)^{-1} = \left[4\frac{x_0}{m}\sum_{i=0}^{m}\frac{1}{\rho^i_{IH}} + (w - 4x_0)\frac{1}{\rho_0}\right] \times \frac{\rho_0}{w} \tag{3}$$

where ρ^i_{IH} is the part of the spatially divided resistivity in the diffuse area taking $2 \times_0$ in consideration of ion diffusion by the ion concentration gradient, which is divided into i, and is given as: $\rho_0 \times 10^{-n^i_{HVO2}}$, where n^i_{HVO2} represents the hydrogen concentration in segment i (i: integral), derived using the finite difference method in equation (2) and the boundary conditions in equation (1). A more detailed derivation is outlined in the Supplementary Information section F.

The experimental results in Fig. 3 are significantly reproduced in Fig. 4b as k_1, k_2 and μ are fitting constants, though the more perfect reproduction requires more consideration efforts in the setting parameters, for example, considering k_1 and k_2 parameters depending on V_G, which make enhanced the reduction rate of resistivity with increasing V_G, and more precise resistive simulation like a random resistor network. Furthermore, this simulation enough includes the important essence of ion diffusion behavior, time and spatial evolutions of the ion diffuse in VO_2 are shown in Fig. 4c,d, which are in the cases at $V_G = 27$ and 38 V, respectively, where $x = 0$ indicates a channel edge. Hydrogen ions expand with time and the concentration increase with increasing V_G. Within the frame work of this model, interestingly, hydrogen ions accumulate in an inner area, clearly observed at $V_G = 38$ V in Fig. 4d. This is caused by the continuous non-equilibrium states of the ion intercalation and diffusion by an electric field. In more detail, this accumulation is induced by the slower ion-diffusion rate in the inner part, depending on deduction of internal electric field with increasing x. As a token of this scenario, following the removal of any V_G, this accumulation fades away in time due to the ion-diffusion by concentration gradient and finally the concentration become homogeneous and equilibrium states. This diffusion behavior at $V_G = 0$ is significantly reproducible for the persisting resistance decrease even after removal of the V_G in Fig. 2a, shown by the simulation in Supplementary Information section G. Thus this device suggests to be a kind of proton pumps in solid-state system.

Drastic resistance modulation in narrower nano-channel. Moreover, this model predict that the magnitude of resistance reduction rate enhance with decreasing the channel width (w) because the effect on the interface diffusion due to the electrochemical gating from lateral sides become more prominent

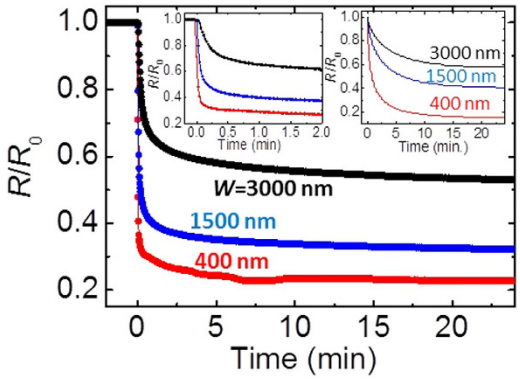

Figure 5. Enhancement of R/R_0 with decreasing w. Time dependence of the simulated R/R_0 values for 400 nm, 1500 nm and 3000 nm wide VO_2 channels at $V_G = 100$ V. The left and right insets show the magnified view of Fig. 5 and the simulation results, respectively.

in narrower w. Figure 5 shows the time dependence of R/R_0 with a variety of wire widths ($w = 400$, 1500 and 3000 nm) at $V_G = 100$ V and 300 K. The saturation values for R/R_0 were enhanced with decreasing w and the sharpness of the resistance deduction in the initial process differs among the three devices as seen in the left inset of Fig. 5, magnified view from 0 to 2 minutes of Fig. 5. This behavior is in agreement with the simulation in the right inset of Fig. 5. Thus the further narrower channel will provide perfect electrochemical gating causing metal-insulator transition in whole channel area.

Discussion

These results show that an air nanogap significantly works as an electrochemical reaction field, even in a gaseous atmosphere, and it is expected that the intercalated elements have an impact on reversibly changing in the physical properties of VO_2. This interfacial effect was more enhanced in smaller nanoscaled channels. This offers a new way to both investigate the fundamental physical properties on the effect of intercalation and non-equilibrium ion diffusion for a wide range of materials and may lead to the realization of new gas-sensing, storage applications and also ion pumps in solid-state materials.

Methods

Thin film growth. 35-nm-thick VO_2 films were prepared on $Al_2O_3(0001)$ single crystal substrates by pulsed laser deposition using an ArF excimer laser at 450 °C under an oxygen pressure of 1.0 Pa. Using X-ray diffraction measurements, it was confirmed that the films were *b*-axis-oriented without any impurity phases.

Device fabrication. The films were patterned into nanowire channels with planer-type field gates by nanoimprint lithography and reactive ion etching using O_2 and SF_6 gases. As advantages of this method, we can easily obtain 200 nm to 400 nm-air gaps between VO_2 gate electrodes and VO_2 channels, and fabricate many PG-FETs at one process. Also, since the resistivity of VO_2 is roughly 1 ohm cm even in insulating region at room temperature, VO_2 gate should enough work as gate electrodes in electrostatic effect. Pt/Cr electrodes were deposited by radio-frequency sputtering. Ohmic contacts between the VO_2 films and electrodes were confirmed.

Electrical measurements. The transport characteristics were measured using a two terminal method with a Keithley 2635A. V_G was applied using a Keithley 236 and the currents between the gate and source electrodes were monitored simultaneously. The temperature of the device was controlled by a Peltier-based temperature stage (T95, Linkam). The gaseous conditions, from dry air to 80% humidity were controlled in a glovebox. The humidity fluctuation was within ±2%.

References

1. Malavasi, L., Mozzati, M. C., Azzoni, C. B., Chiodelli, G. & Flor, G. Role of oxygen content on the transport and magnetic properties of $La_{1-x}Ca_xMnO_{3+\delta}$ manganites. *Solid State Commun.* **123,** 321–326 (2002).
2. Nagashima, M., Wada, H., Tanikawa, K. & Shirahata, H. The electronic behaviors of oxygen-deficient VO_2 thin films in low temperature region. *Jpn. J. Appl. Phys.* **37,** 4433–4438 (1998).
3. Zhao, Y. *et al.* Electrical transport and magnetic properties of $La_{0.5}Ca_{0.5}MnO_{3-y}$ with varying oxygen content. *Phys. Rev. B* **65,** 144406 (2002).
4. Poulsen, F. Defect chemistry modelling of oxygen-stoichiometry, vacancy concentrations, and conductivity of $(La_{1-x}Sr_x)_yMnO_{3\pm\delta}$. *Solid State Ionics* **129,** 145–162 (2000).
5. Wu, J. *et al.* Strain-Induced Self Organization of Metal-Insulator Domains in Single-Crystalline VO_2 Nanobeams. *Nano Lett.* **6,** 2313–2317 (2006).
6. Cheng, C. *et al.* Heat Transfer across the Interface between Nanoscale Solids and Gas. *ASC Nano* **5,** 10102–10107 (2011).

7. Pellegrino, L. *et al.* Multistate Memory Devices Based on Free-standing VO_2/TiO_2 Microstructures Driven by Joule Self-Heating. *Adv. Mater.* **24,** 2929–2934 (2012).
8. Cheng, C., Liu, K., Xiang, B., Suh, J. & Wu, J. Ultra-long, free-standing, single-crystalline vanadium dioxide micro/nanowires grown by simple thermal evaporation. *Appl. Phys. Lett.* **100,** 103111 (2012).
9. Manca, N. *et al.* Programmable Mechanical Resonances in MEMS by Localized Joule Heating of Phase Change Materials. *Adv. Mater.* **25,** 6430–6435 (2013).
10. Cheng, C. *et al.* Self-Assembly and Horizontal Orientation Growth of VO_2 Nanowires. *Sci. Rep.* **4,** 5456 (2014).
11. Takami, H., Kanki, T. & Tanaka, H. Multistep metal insulator transition in VO_2 nanowires on $Al_2O_3(0001)$ substrates. *Appl. Phys. Lett.* **104,** 023104 (2014).
12. Guo, H. *et al.* Vanadium dioxide nanowire-based microthermometer for quantitative evaluation of electron beam heating. *Nat. Commun.* **5,** 4986 (2015).
13. Matsui, H. *et al.* Mid-infrared Plasmonic Resonances in 2D VO_2 Nanosquare Arrays. *Adv. Opt. Mater.* In-press doi: 10.1002/adom.201500322.
14. Wei, J., Ji, H., Guo, W., Nevidomskyy, A. H. & Natelson, D. Hydrogen stabilization of metallic vanadium dioxide in single-crystal nanobeams. *Nat. Nanotechnol.* **7,** 357–362 (2012).
15. Pan, X., Zhao, Y., Ren, G. & Fan, Z. Highly conductive VO_2 treated with hydrogen for supercapacitors. *Chem. Commun. (Camb).* **49,** 3943 (2013).
16. Hong, W. *et al.* Hydrogen-induced morphotropic phase transformation of single-crystalline vanadium dioxide nanobeams. *Nano Lett.* 13, 1822 (2013).
17. Andreev, V. N., Kapralova, V. M. & Klimov, V. A. Effect of hydrogenation on the metal-semiconductor phase transition in vanadium dioxide thin films. *Phys. Solid State* **49,** 2318–2322 (2007).
18. Andreev, V. N., Klimov, V. A. & Kompan, M. E. Influence of hydrogenation on electrical conductivity of vanadium dioxide thin films. *Phys. Solid State* **54,** 601–606 (2012).
19. Filinchuk, Y. *et al. In situ* diffraction study of catalytic hydrogenation of VO_2: Stable phases and origins of metallicity. *J. Am. Chem. Soc.* **136,** 8100–8109 (2014).
20. Sim, J. S., Zhou, Y. & Ramanathan, S. Suspended sub-50 nm vanadium dioxide membrane transistors: fabrication and ionic liquid gating studies. *Nanoscale* **4,** 7056–7062 (2012).
21. Ji, H., Wei, J. & Natelson, D. Modulation of the electrical properties of VO_2 nanobeams using an ionic liquid as a gating medium. *Nano Lett.* **12,** 2988–2992 (2012).
22. Jeong, J. *et al.* Suppression of metal-insulator transition in VO_2 by electric field-induced oxygen vacancy formation. *Science* **339,** 1402–1405 (2013).
23. Liu, K. *et al.* Dense electron system from gate-controlled surface metal-insulator transition. *Nano Lett.* **12,** 6272–6277 (2012).
24. Ohta, H. *et al.* Field-induced water electrolysis switches an oxide semiconductor from an insulator to a metal. *Nat. Commun.* **1,** 118 (2010).
25. Ruzmetov, D. *et al.* Three-terminal field effect devices utilizing thin film vanadium oxide as the channel layer. *J. Appl. Phys.* **107,** 114516 (2010).
26. Zhou, Y. & Ranamanathan, S. Relaxation dynamics of ionic liquid – VO_2 interfaces and influence in electric double-layer transistors. *J. Appl. Phys.* **111,** 084508 (2012).
27. Sengupta, S. *et al.* Field-effect modulation of conductance in VO_2 nanobeam transistors with HfO_2 as the gate dielectric. *Appl. Phys. Lett.* **99,** 062114 (2011).
28. Ruzmetov, D. *et al.* Hall carrier density and magnetoresistance measurements in thin-film vanadium dioxide across the metal-insulator transition. *Phys. Rev. B* **79,** 153107 (2009).
29. Yuan, H. *et al.* Hydrogenation-induced surface polarity recognition and proton memory behavior at protic-ionic-liquid/oxide electric-double-layer interfaces. *J. Am. Chem. Soc.* **132,** 6672–6678 (2010).
30. Shi, J., Zhou, Y. & Ramanathan, S. Colossal resistance switching and band gap modulation in a perovskite nickelate by electron doping. *Nat. Commun.* **5,** 4860 (2014).
31. Mortimer, R. J. Electrochromic Materials. *Annu. Rev. Mater. Res.* **41,** 241–68 (2011).
32. Yang, Z. *et al.* Dielectric and carrier transport properties of vanadium dioxide thin films across the phase transition utilizing gated capacitor devices. *Phys. Rev. B* **82,** 205101 (2010).
33. Zhu, B. & Mellander, B.-E. fProton conduction and diffusion in Li_2SO_4. *Solid State Ionics* **97,** 535–540 (1997).

Acknowledgements

This work was supported by a Grant-in-Aid for Scientific Research A (No. 26246013), a Grant-in-Aid for Scientific Research B (No. 25286058) from the Japan Society for the Promotion of Science (JSPS) and the Nanotechnology Platform Project (Nanotechnology Open Facilities in Osaka University) from the Ministry of Education, Culture, Sports, Science and Technology, Japan (MEXT) (F-14-OS-0010, S-14-OS-0007).

Author Contributions

T.S. fabricated the devices, conducted the measurements and analyzed the data. H.U. contributed to the nanofabrication processes used to prepare the devices and the experimental setup. T.K. and H.T. planned and supervised the research. T.S., T.K. and H.T wrote the manuscript. All authors discussed the results.

Additional Information

Supplementary information accompanies this paper at http://www.nature.com/srep

Competing financial interests: The authors declare no competing financial interests.

How to cite this article: Sasaki, T. *et al.* Electrochemical gating-induced reversible and drastic resistance switching in VO_2 nanowires. *Sci. Rep.* **5**, 17080; doi: 10.1038/srep17080 (2015).